Imaging Methods

DOI: 10.1002/anie.201002830

Scanning Imaging of Magnetic Nanoparticles for Quantitative Molecular Imaging**

*Li Yao, Andrew C. Jamison, and Shoujun Xu**

Molecular imaging is a powerful tool for studying chemical and biomedical processes with high specificity and minimal background interference.[1] A variety of imaging methods enjoy widespread use, including those based on fluorescence, radioactivity, and magnetism.[2] Whilst each labeling method offers advantages and disadvantages, magnetic labeling stands out because of its low toxicity, noninvasive detection, facile manipulation with an external magnetic field, and potential therapeutic uses.[3]

Imaging of magnetically-labeled molecules, particularly under in vivo conditions, has broad impact in drug delivery, medical diagnosis, cellular imaging, and hyperthermia treatment for cancers.[4] To achieve this goal, highly sensitive imaging with a long detection range is needed. The requirement of an extended detection range rules out most microscopic techniques.[5] Whilst many technologies have been developed,[6] magnetic resonance imaging (MRI) is the current technology of choice owing to its high spatial resolution and reasonable detection limit.[7] MRI, however, is not a direct measuring technique for magnetic particles because the inductive detection of MRI is not responsive to direct current magnetic fields.[8]

Recently, we reported an innovative scanning imaging technique with a detection range of nearly one centimeter.[9] It utilizes a sensitive atomic magnetometer, which uses coherent alkali atoms to measure magnetic fields, coupled with a scanning imaging system to obtain a magnetic field profile instead of a single-point measurement. This technique is able to simultaneously reveal spatial information and the quantity of magnetic particles in a given sample volume. Until now, the spatial resolution of this technique was limited to one dimension, and no examples of molecular imaging were demonstrated.

Herein we demonstrate two-dimensional imaging of arbitrarily oriented magnetic nanoparticles and quantitative molecular imaging of a targeted antibody. A linear response is revealed for a wide range of sample quantities. Scanning electron microscopy is used to confirm the binding of α-antibody molecules labeled with magnetic nanoparticles onto immobilized antibodies. We also show that three-dimensional scanning magnetic imaging is achievable.

When two samples consisting of magnetic particles are present, each with an arbitrary magnetic orientation, the magnetic field from each sample along the detection axis of a vector atomic magnetometer is given by Equation (1):

$$B_i = \frac{\mu_0 M_i}{4\pi((x-x_i)^2+d_i^2)^{3/2}}\left(\frac{3a_i d_i^2}{(x-x_i)^2+d_i^2}+3\sqrt{1-a_i^2}\,\frac{(x-x_i)d_i}{(x-x_i)^2+d_i^2}-a_i\right) \quad (1)$$

As shown in Figure 1 a, d_i and x_i represent the coordinates of the corresponding sample, with $i = 1, 2$. The d axis is the detection axis of the vector magnetometer. The variable x is the position during the scan, M_i is the total magnetization of the sample, and a_i is equal to $\cos\theta_i$, where θ_i is the angle between the magnetic orientation of the corresponding sample and the d axis.

Two magnetic samples with equal quantities of amine-coated magnetic particles were located on a sample holder, with a distance of 0.100 ± 0.005 mm along the d axis and 40.0 ± 0.2 mm along the x axis. A magnetic field profile was obtained when the sample holder was scanned along the x axis, which revealed the d_i and x_i values of the two samples. The coordinates of the two samples were $(6.677 \pm 0.019, 66.47 \pm 0.01)$ and $(6.779 \pm 0.024, 106.77 \pm 0.02)$ mm, respectively. Therefore, the distances measured by scanning magnetic imaging were 0.102 mm along the d axis and 40.30 mm along the x axis. The widths of the traces represent the respective fitting errors of d_i (Figure 1 b).

To demonstrate the accuracy of the two-dimensional positions of the samples, a series of five scans were performed by sequentially increasing the d coordinate by 0.100 mm using translation stages. The fitted d coordinates of the two samples were then offset by the corresponding stage movement. The results are shown in Figure 1 c. For each scan, the d coordinate difference is 0.100 ± 0.007 mm and the x coordinate difference is 40.0 ± 0.3 mm (see Supporting Information, Table S1, for details). Furthermore, the fitted magnetizations of the samples, M_i, are within 6% for all of the scans; the accuracy of the relative amount, M_1/M_2, is better than 3%.

To correlate the measured magnetization with the amount of magnetic sample, we studied the magnetization as a function of the amount (by mass) of the magnetic particles. A specified amount of magnetic particles was scanned along the x axis; the resulting magnetic profiles provided the corresponding magnetization values (see Supporting Information,

[*] Dr. L. Yao, A. C. Jamison, Prof. S. Xu
Department of Chemistry, University of Houston
Houston, TX 77204 (USA)
Fax: (+1) 713-743-2709
E-mail: sxu7@uh.edu
Homepage: http://www.chem.uh.edu/Faculty/Xu/

[**] This work was supported in part by a GEAR grant and the Texas Center of Superconductivity at the University of Houston. L.Y. acknowledges support by the McElrath Fellowship. We thank Prof. Haibing Peng for assistance in obtaining the SEM images, and Prof. T. Randall Lee for helpful discussions and access to his laboratory resources.

Supporting information for this article is available on the WWW under http://dx.doi.org/10.1002/anie.201002830.

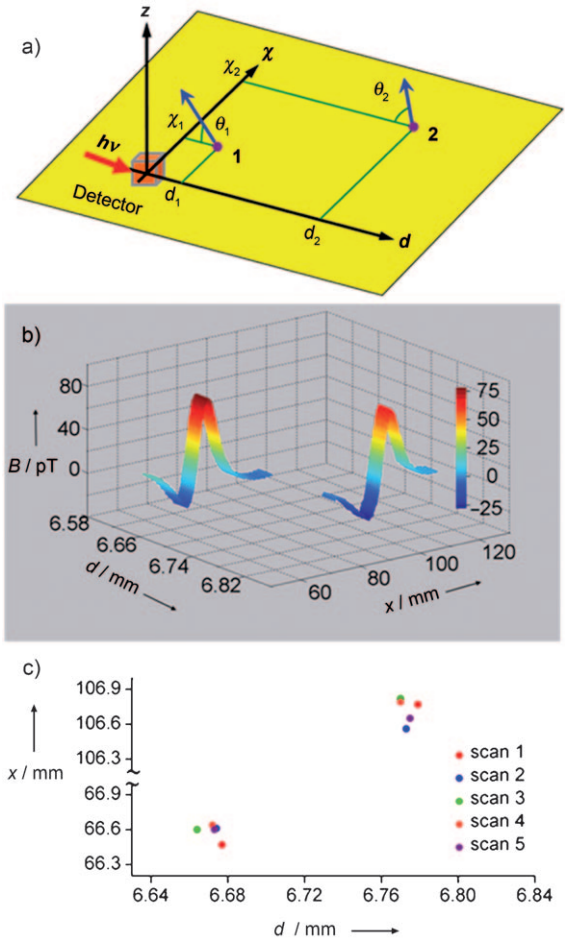

Figure 1. Two-dimensional scanning magnetic imaging. a) Geometry of the two samples, which were separated by 0.100 mm along the *d* axis (d_2-d_1) and 40.0 mm along the *x* axis (x_2-x_1). The *d* axis is the detection axis of the vector atomic magnetometer (shown as a cube with the laser beam propagating along the *d* axis), and the *x* and *z* axes are perpendicular to the detection axis. θ_i is the angle between the magnetization of the respective sample and the *d* axis. b) A scanning magnetic profile of the two samples, plotted against respective fitted *d* values and *x* scan positions. c) Five images overlaid to show the spatial accuracy on both the *d* and the *x* axes.

Figure S1). Figure 2a shows the data obtained from the same samples used in the two-dimensional imaging. The data indicate that the obtained magnetization is proportional to the mass of the particles. Furthermore, the dynamic range of the linear response is nearly three orders of magnitude. Such a wide response range facilitates applications in biological separation and molecular imaging, where the concentration of the targeted molecules can vary substantially.

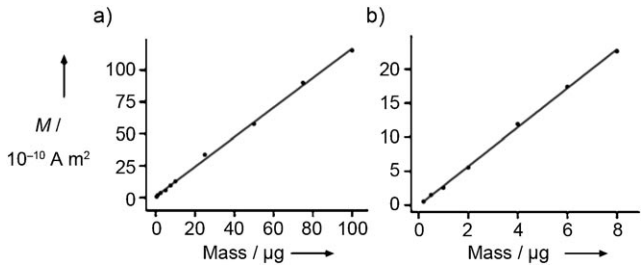

Figure 2. Quantification of magnetization *M* of magnetic nanoparticles. *M* is obtained from scanning magnetic imaging as a function of the mass of magnetic particles. a) Amine-coated magnetic particles. b) Magnetic particles coated with goat α-mouse IgG.

In the current configuration, the upper detection limit of our atomic magnetometer is governed by the width of the magneto-optical resonance, which is about 50 Hz. Given that the gyromagnetic ratio of cesium is 7 Hz/nT, we estimate the upper limit to be 7 nT. The lower limit is determined by the sensitivity, which is about 150 fT for a one-second integration time. These two limits define a dynamic range of more than four orders of magnitude, which is a significant advantage over competing detection technologies based, for example, on giant magnetoresistive sensors.[10] Furthermore, the sensitivity of atomic magnetometers is amenable to improvement.[11] For our magnetometer specifically, the sensitivity can ultimately reach less than 1 fT,[12] which will extend the dynamic range even further.

For quantitative molecular imaging, we first measured magnetization against sample amount for another kind of magnetic nanoparticles, which was labeled with goat α-mouse IgG (Figure 2b). The data in Figure 2b also show that the magnetization is proportional to the amount of the particles present; the slope is different from the amine-coated magnetic particles owing to their differences in intrinsic magnetic properties.

Using scanning magnetic imaging, we investigated the binding of magnetic particles coated with goat α-mouse IgG onto mouse IgG immobilized on a gold surface (Figure 3).[13] The profile for the gold surface shows a non-magnetic background (Figure 3a). To ensure the removal of physisorbed magnetic particles, we developed a washing procedure and examined the results (Figure 3b). The magnetic profile confirmed that the interference from the physisorbed magnetic particles is negligible after washing. Two separate 5 μL aliquots of magnetic particles at concentrations of 0.5 $mg\,mL^{-1}$ and 1.0 $mg\,mL^{-1}$ were respectively incubated with the mouse IgG-coated gold surface and washed using the established procedure. The results are shown in Figure 3c,d. For the 0.5 $mg\,mL^{-1}$ solution, the fitted magnetization corresponds to 0.93 μg of bound particles based on the calibration curve shown in Figure 2b, which contains 9.3×10^4 particles according to the manufacturer's specification. This amount is comparable to the detection limit of a superconducting quantum interference device with a 40 μm detection distance.[14] Our technique, however, offers a circa 9 mm detection distance: the distance between the surface and the detector is 8.755 ± 0.109 mm. The data for the 1.0 $mg\,mL^{-1}$ solution revealed that the bound particles increased to 3.0 μg, which is equivalent to 3.0×10^5 particles. The distance is 8.591 ± 0.024 mm. Combining the fitted *x* and *d* values with the quantities, we obtained corresponding images (Figure 3e–h). The coordinates are (131.99 ± 0.048, 7.991 ± 0.129), (129.71 ± 0.148, 8.755 ± 0.109), and (134.07 ± 0.027, 8.591 ± 0.024) mm for Figure 3f, g, and h respectively. Figure 3e is blank because of the absence of bound particles. The gray scale of the sample dots indicates the quantity of the particles, with a darker filling indicating a higher quantity. Each pair of

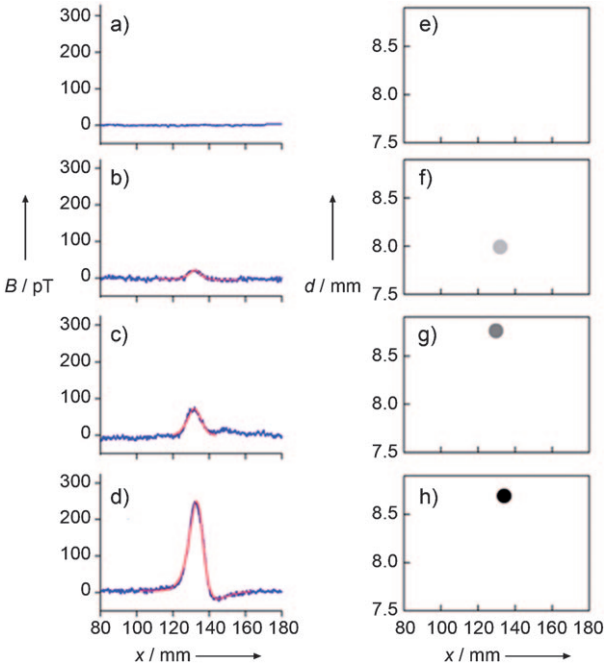

Figure 3. Quantitative molecular imaging: a–d) Scanning magnetic field profiles and e–h) the resulting images. a,e) Background: measurement of gold-coated substrate prior to antibody immobilization. b,f) Control: binding of 1.0 mg mL^{-1} IgG magnetic nanoparticles to unmodified gold-coated substrate. c,g) Binding of 0.5 mg mL^{-1} magnetic nanoparticles to antibody-coated substrate. d,h) Binding of 1.0 mg mL^{-1} magnetic nanoparticles to antibody-coated substrate. Panels (b), (c), and (d) show the fits (red traces) used to extract the magnetization values and spatial information.

coordinates represents the mounting position of the corresponding sample after the incubation and washing procedure, which is not necessarily exactly the same as the previous position. It is interesting to note that by increasing the concentration by a factor of two, the binding proportion was improved from 37% to 60%.

Scanning electron microscopy (SEM) was employed to provide complementary data for the above-mentioned four steps (see Supporting Information, Figure S2). No particles were observed in the background test, and few were detected in the control test. When the targeted antibody molecules were present on the gold surface, the corresponding images show magnetic particles present for the 0.5 mg mL^{-1} solution, and a greater number of particles for the 1.0 mg mL^{-1} solution. We thus conclude that the SEM images are consistent with the results obtained using scanning magnetic imaging.

To further validate the quantities of the magnetic particles, we took an optical image of the sample in Figure 3b and statistically counted the number of particles (see Supporting Information, Figure S3). The counting yields 2.1×10^4 particles, which agrees well with the fitting result from scanning magnetic imaging of 2.3×10^4 in Figure 3f. We chose this sample for comparison because it was possible to directly count the number of particles owing to the low density and hence no overlapping. The advantage of scanning magnetic imaging is that it gives precise measurement when direct optical techniques are not applicable, which is often the case in molecular imaging applications.

Our technique can be expanded to three-dimensional imaging. As the z axis (Figure 1a) is equivalent to the x axis as both axes are perpendicular to the detection axis d, scanning along the z axis in addition to scanning along the x axis will achieve three-dimensional imaging. With further improvement in sensitivity and scanning schemes, a sub-millimeter spatial resolution on three dimensions can be achieved and the detection range can be extended. For example, from the projected sensitivity of sub-femtotesla,[12] the detection range will be about 5 cm based on the r^{-3} dependence of the signal, which will be a significant advantage over optical imaging. Furthermore, our technique has a relatively low background signal because only the magnetic particles can provide a detectable signal, whilst optical techniques need to overcome undesired scattering, optical interference, and auto fluorescence.[15]

In summary, we have demonstrated two-dimensional scanning magnetic imaging of functionalized magnetic nanoparticles and quantitative molecular imaging. The long detection range distinguishes our method from existing microscopic techniques, making it uniquely suitable for practical molecular imaging. As absolute magnetization is measured, the quantity of the magnetic entities can be directly revealed without interference from experimental settings. With further development, both on the technical front and in the data processing, our method will be valuable for quantitative molecular imaging in complex practical situations, which is a key to the success of nanomedicine.

Experimental Section

The atomic magnetometer has a sensitivity of about 150 fT/(Hz)$^{1/2}$.[16] The motion of the samples was achieved by using an automated linear actuator for x-axis scans and a pair of motorized positioning stages for d-axis movements. The magnetic field was measured with an integration time of 30 ms for each data point. More experimental details are provided in the Supporting Information.

Received: May 10, 2010
Revised: June 25, 2010
Published online: August 30, 2010

Keywords: antibodies · magnetic nanoparticles · magnetometry · molecular imaging · nanotechnology

[1] a) A. D. Waldman, A. Jackson, S. J. Price, C. A. Clark, T. C. Booth, D. P. Auer, P. S. Tofts, D. J. Collins, M. O. Leach, J. H. Rees, *Nat. Rev. Clin. Oncol.* **2009**, *6*, 445–454; b) S. Y. Shaw, *Nat. Rev. Cardiol.* **2009**, *6*, 569–579; c) D. R. Elias, D. L. J. Thorek, A. K. Chen, J. Czupryna, A. Tzourkas, *Cancer Biomarkers* **2008**, *4*, 287–305; d) F. Pouliot, M. Johnson, L. Wu, *Trends Mol. Med.* **2009**, *15*, 254–262.

[2] a) D. Rugar, R. Budakian, H. J. Mamin, B. W. Chui, *Nature* **2004**, *430*, 329–332; b) U. Kaiser, A. Schwarz, R. Wiesendanger, *Nature* **2007**, *446*, 522–525; c) S. Schreiber, M. Salva, D. V. Pelekhov, D. F. Iscru, C. Selcu, P. C. Hammel, G. Agarwal, *Small* **2008**, *4*, 270–278; d) B. Huang, W. Wang, M. Bates, X. Zhuang, *Science* **2008**, *319*, 810–813; e) M. Fernández-Suárez, A. Y. Ting, *Nat. Rev. Mol. Cell Biol.* **2008**, *9*, 929–943.

[3] a) H. Jadvar, *Nat. Rev. Urol.* **2009**, *6*, 317 – 323; b) M. De Jong, W. A. P. Breeman, D. J. Kwekkeboom, R. Valkema, E. P. Krenning, *Acc. Chem. Res.* **2009**, *42*, 873 – 880.
[4] a) R. D. K. Misra, *Mater. Sci. Technol.* **2008**, *24*, 1011 – 1019; b) C. Leuschner, C. S. Kumar, W. Hansel, W. Soboyejo, J. Zhou, J. Hormes, *Breast Cancer Res. Treat.* **2006**, *99*, 163 – 176.
[5] a) J. W. M. Bulte, *AJR Am. J. Roentgenol.* **2009**, *193*, 314 – 325; b) J.-M. Nam, C. S. Thaxton, C. A. Mirkin, *Science* **2003**, *301*, 1884 – 1886; c) A. Ito, M. Shinkai, H. Honda, T. Kobayashi, *J. Biosci. Bioeng.* **2005**, *100*, 1 – 11.
[6] a) B. Gleich, J. Weizenecker, *Nature* **2005**, *435*, 1214 – 1217; b) D. Baumgarten, M. Liehr, F. Wiekhorst, U. Steinhoff, P. Münster, P. Miethe, L. Trahms, J. Haueisen, *Med. Biol. Eng. Comput.* **2008**, *46*, 1177 – 1185.
[7] a) U. Himmelreich, T. Dresselaers, *Methods* **2009**, *48*, 112 – 124; b) R. Kopelman, Y.-E. L. Koo, M. Philbert, B. A. Moffat, G. R. Reddy, P. McConville, D. E. Hall, T. L. Chenevert, M. S. Bhojani, S. M. Buck, A. Rehemtulla, B. D. Ross, *J. Magn. Magn. Mater.* **2005**, *293*, 404 – 410.
[8] E. Harel, L. Schröder, S.-J. Xu, *Annu. Rev. Anal. Chem.* **2008**, *1*, 133 – 163.
[9] L. Yao, S.-J. Xu, *Angew. Chem.* **2009**, *121*, 5789 – 5792; *Angew. Chem. Int. Ed.* **2009**, *48*, 5679 – 5682.
[10] J. Nordling, R. L. Millen, H. A. Bullen, M. D. Porter, *Anal. Chem.* **2008**, *80*, 7930 – 7939.
[11] a) D. Budker, M. V. Romalis, *Nat. Phys.* **2007**, *3*, 227 – 234; b) I. K. Kominis, T. W. Kornack, J. C. Allred, M. V. Romalis, *Nature* **2003**, *422*, 596 – 599; c) D. Yu, N. Garcia, S.-J. Xu, *Concepts Magn. Reson. Part A* **2009**, *34*, 124 – 132.
[12] V. Shah, S. Knappe, P. D. D. Schwindt, J. Kitching, *Nat. Photonics* **2007**, *1*, 649 – 652.
[13] R. L. Millen, T. Kawaguchi, M. C. Granger, M. D. Porter, M. Tondra, *Anal. Chem.* **2005**, *77*, 6581 – 6587.
[14] Y. R. Chemla, H. L. Crossman, Y. Poon, R. McDermott, R. Stevens, M. D. Alper, J. Clarke, *Proc. Natl. Acad. Sci. USA* **2000**, *97*, 14268 – 14272.
[15] Y. Koyama, T. Barrett, Y. Hama, G. Ravizzini, P. L. Choyke, H. Kobayashi, *Neoplasia* **2007**, *12*, 1021 – 1029.
[16] N. C. Garcia, D. Yu, L. Yao, S.-J. Xu, *Opt. Lett.* **2010**, *35*, 661 – 663.

